

nature

NAME THAT ATOM

Individual surface
atoms identified
by atomic force
microscopy

GRAPHENE

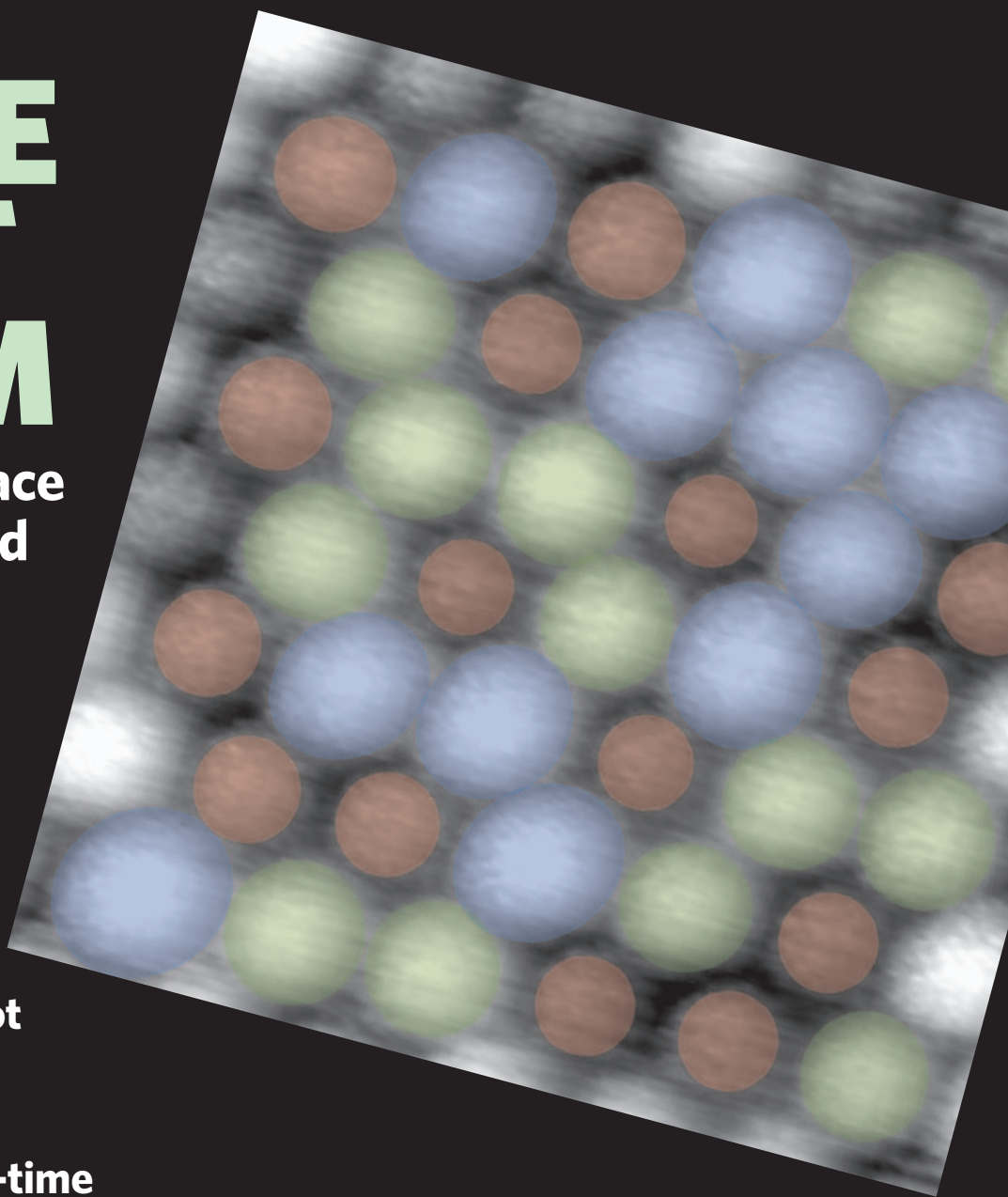
What makes this hot
new material tick?

EXTREME LASERS

Letting rip in space-time

CYPAVIRUS POLYHEDRA

Small but perfectly formed



NATUREJOBS

Focus on physics



LETTERS

Chemical identification of individual surface atoms by atomic force microscopy

Yoshiaki Sugimoto¹, Pablo Pou², Masayuki Abe^{1,3}, Pavel Jelinek⁴, Rubén Pérez², Seizo Morita¹ & Óscar Custance¹

Scanning probe microscopy is a versatile and powerful method that uses sharp tips to image, measure and manipulate matter at surfaces with atomic resolution^{1,2}. At cryogenic temperatures, scanning probe microscopy can even provide electron tunnelling spectra that serve as fingerprints of the vibrational properties of adsorbed molecules^{3–5} and of the electronic properties of magnetic impurity atoms^{6,7}, thereby allowing chemical identification. But in many instances, and particularly for insulating systems, determining the exact chemical composition of surfaces or nanostructures remains a considerable challenge. In principle, dynamic force microscopy should make it possible to overcome this problem: it can image insulator, semiconductor and metal surfaces with true atomic resolution^{8–10}, by detecting and precisely measuring^{11–13} the short-range forces that arise with the onset of chemical bonding between the tip and surface atoms^{14,15} and that depend sensitively on the chemical identity of the atoms involved. Here we report precise measurements of such short-range chemical forces, and show that their dependence on the force microscope tip used can be overcome through a normalization procedure. This allows us to use the chemical force measurements as the basis for atomic recognition, even at room temperature. We illustrate the performance of this approach by imaging the surface of a particularly challenging alloy system and successfully identifying the three constituent atomic species silicon, tin and lead, even though these exhibit very similar chemical properties and identical surface position preferences that render any discrimination attempt based on topographic measurements impossible.

The chemical identification of single atoms and molecules at surfaces has been pursued since the invention of both the scanning tunnelling microscope and the atomic force microscope (AFM). Particularly promising in this quest is dynamic force microscopy, which achieves true atomic imaging resolution^{8–10} by detecting the short-range forces associated with the onset of the chemical bond between the outermost atom of the tip apex and the surface atoms being imaged^{14,15} (see Fig. 1 for schematic illustration of the method and imaging examples). Moreover, dynamic force spectroscopy^{11–13} makes it possible to quantify these forces.

Figure 2a shows five sets of dynamic force spectra measured on a single atomic layer of Sn grown on a Si(111) substrate. Each set of force curves was obtained over an Sn atom and an Si atom having the same local surface configuration as the corresponding atoms highlighted in the topographic image shown in Fig. 1d, always using identical acquisition and analysis protocols (see Methods). However, the sets were collected over multiple measurement sessions, using tips that had different apex terminations. These tip apexes presumably differ in both structure and composition (Sn or Si), as sometimes slight tip–surface contacts were intentionally produced before the acquisition of each set of force curves. The sets seem to share only

one feature: curves measured over the Si atoms are characterized by a stronger attractive interaction force. Given the high degree of stability, lateral positioning accuracy, and reproducibility provided by our acquisition protocol^{12,16}, we attribute the variability seen in the data in Fig. 2a to a strong tip dependence of both the registered

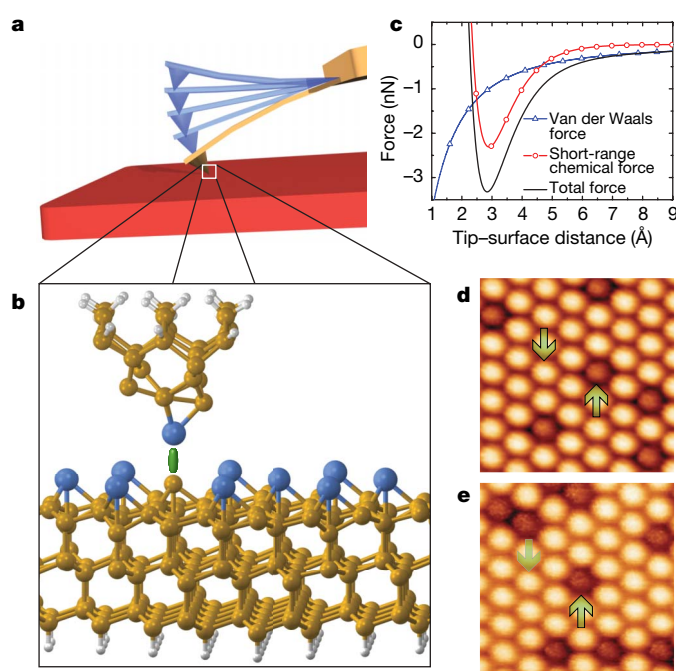


Figure 1 | Dynamic force microscopy with atomic resolution. Schematic illustration of AFM operation in dynamic mode (a), and of the onset of the chemical bonding between the outermost tip atom and a surface atom (highlighted by the green stick) that gives rise to the atomic contrast^{14,15} (b). However, the tip experiences not only the short-range force associated with this chemical interaction, but also long-range force contributions that arise from van der Waals and electrostatic interactions between tip and surface (though the effect of the latter is usually minimized through appropriate choice of the experimental set-up). c, Curves obtained with analytical expressions for the van der Waals force, the short-range chemical interaction force, and the total force to illustrate their dependence on the absolute tip–surface distance. d–e, Dynamic force microscopy topographic images of a single-atomic layer of Sn (d) and Pb (e) grown, respectively, over a Si(111) substrate. At these surfaces, a small concentration of substitutional Si defects, characterized by a diminished topographic contrast²⁰, is usually found. The green arrows indicate atomic positions where force spectroscopic measurements were performed (see Fig. 2). Image dimensions are (4.3×4.3) nm²; for the acquisition parameters see the Supplementary Information.

¹Graduate School of Engineering, Osaka University, 2-1 Yamada-Oka, 565-0871 Suita, Osaka, Japan. ²Departamento de Física Teórica de la Materia Condensada, Universidad Autónoma de Madrid, 28049 Madrid, Spain. ³PRESTO, Japan Science and Technology Agency, Saitama 332-0012, Japan. ⁴Institute of Physics, Academy of Sciences of the Czech Republic, Cukrovarnická 10, 1862 53, Prague, Czech Republic.

maximum attractive force value and the distance dependence of the attractive and repulsive regions of the curves.

A meaningful comparison of measured short-range forces requires some data processing to reduce the variability caused by the use of tips with different terminations. We have found that the relative interaction ratio, that is, the ratio of the maximum attractive short-range forces of the two curves within a set of measurements over Si and Sn (acquired using a tip that had the same apex termination), remains nearly constant. This is illustrated in Fig. 2b, where each curve within a given measurement set has been normalized to the absolute value of the maximum attractive short-range force of the Si curve of that set ($|F_{\text{Si(set)}}|$). The normalization reveals an average value for the relative interaction ratio of 0.77 ± 0.02 . This approach has also been validated for elements such as Pb or In in similar surfaces (see Fig. 1e, Fig. 2c, d and Supplementary Information). Using the same acquisition and analysis protocols as applied when studying the mixed Sn/Si surface layer, several sets of short-range force curves were obtained over structurally equivalent atoms (for the Pb/Si layer, these are highlighted by arrows in Fig. 1e). The data revealed an average relative interaction ratio of 0.59 ± 0.03 for Pb and Si in the Pb-terminated surface (Fig. 2c, d), and an average relative interaction ratio for In and Si of 0.72 ± 0.04 in the In-terminated one.

To corroborate the experimental observations, we conducted large-scale first-principles calculations (see Methods) using atomically extended nanometre-scale asperities¹⁷ as tip-apex models. In these calculations, homogeneous tip apexes that have different structures for probing the Sn and Si atoms of a model of the mixed Sn/Si surface layer (shown in Fig. 1b) produce different short-range force curves (Fig. 2e). If the tip apexes have the same termination structure but a different element at the outermost position, we obtain weaker short-range forces for Sn-terminated tips than for Si-terminated tips (Fig. 2e). In all these cases, as in the experiments, the tip-surface interaction is stronger over Si surface atoms than over Sn atoms (Fig. 2e). But independently of tip-apex structure and the chemical termination of the tips, the relative interaction ratios of the

maximum attractive forces calculated over the Sn and Si atoms for a given tip are all similar, with an average value of 0.71 ± 0.07 (Fig. 2f) that is close to the experimental ratio.

To gain some insight into the behaviour of the short-range forces, we have developed a simple analytical model that assumes that tip and sample deform elastically in response to the short-range chemical interaction between the tip apex and the closest surface atoms (P.P., Y.S., P.J., M.A., S.M., O.C. and R.P., manuscript in preparation). The model indicates that although the shape of the force-versus-distance curves depends on the elastic response of the system, the value of the maximum attractive short-range force is determined only by the short-range chemical interaction (data not shown). The minimum short-range force value registered for a given surface atom (corresponding to maximum attractive force) is thus expected to depend significantly on the chemical composition and structure of the tip apex (an effect seen in the data in Fig. 2e), and will also depend on the relative orientation of the tip with respect to the surface^{18,19}. These three factors explain the strong tip dependence found in the experiments (see Fig. 2a and c). However, when the relative interaction ratio of the maximum attractive short-range forces for two atomic species probed with the same tip is considered, the common features associated with the structural characteristics of the tip-apex cancel out, and the intrinsic strength of the chemical bonding interaction between the outermost tip atom and the closest surface atom is revealed (Fig. 2b, d and f). This explanation can be rationalized for semiconductor surfaces using accepted combination rules for covalent chemical interactions; it can, in fact, be generalized to multi-element systems by considering that when individually probing the atoms of such systems with a given tip apex, interactions between pairs of atomic species are obtained. This ensures that the relative strengths of the minimum short-range forces are almost independent from the tip-apex structure or chemical termination (see Supplementary Information for further details).

By determining the ratio of the maximum attractive short-range forces as outlined above, it is possible to identify individual atoms in

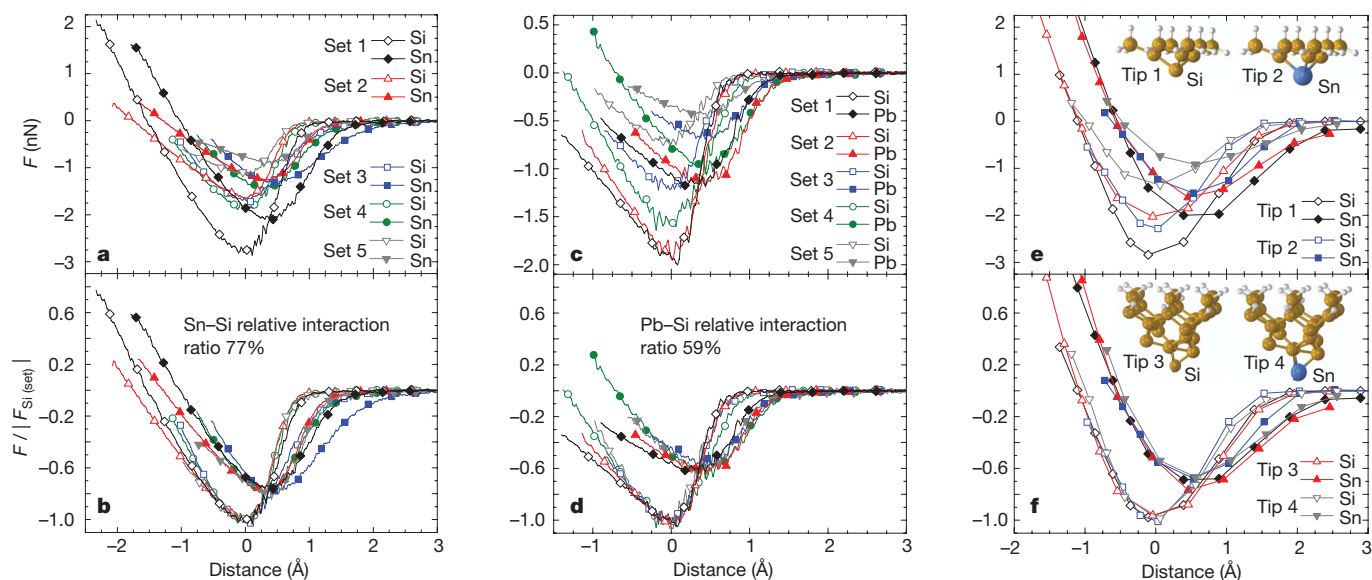


Figure 2 | Probing short-range chemical interaction forces. **a**, Sets of short-range force curves obtained over structurally equivalent Sn and Si atoms. All curves are obtained using identical acquisition and analysis protocols, but the tips differ from set to set. **b**, The same force curves as in **a**, but the curves in each set are now normalized to the absolute value of the minimum short-range force of the Si curve ($|F_{\text{Si(set)}}|$). **c**, **d**, Sets of short-range force curves for Pb and Si, obtained in the same way as for Sn and Si, before (**c**) and after (**d**) normalization. The average relative interaction ratios calibrated against Si, or the maximum attractive short-range forces for Sn and Pb relative to those of Si (77% and 59%, respectively), provide an intrinsic signature for

the chemical identification of individual atoms. Each experimental force characteristic shown here was obtained from the measurement of a hundred spectroscopic curves (see Methods for details). The acquisition parameters are available in the Supplementary Information. **e**, **f**, Chemical force curves calculated for different tip-apex models (see insets for structural and chemical characteristics) over the Sn and Si atoms of the $(\sqrt{3} \times \sqrt{3})$ R30° surface model shown in Fig. 1b. The curves are shown before (**e**) and after (**f**) normalization. In both the experimental and the calculated short-range force curves, the distance axes denote the tip-sample relative displacement (see Methods for details).

multi-element systems. This capability of the AFM is demonstrated in Fig. 3, where we have unambiguously discriminated between the three species—topographically not clearly distinguishable—of a surface alloy comprised of Si, Sn, and Pb atoms mixed in equal proportions

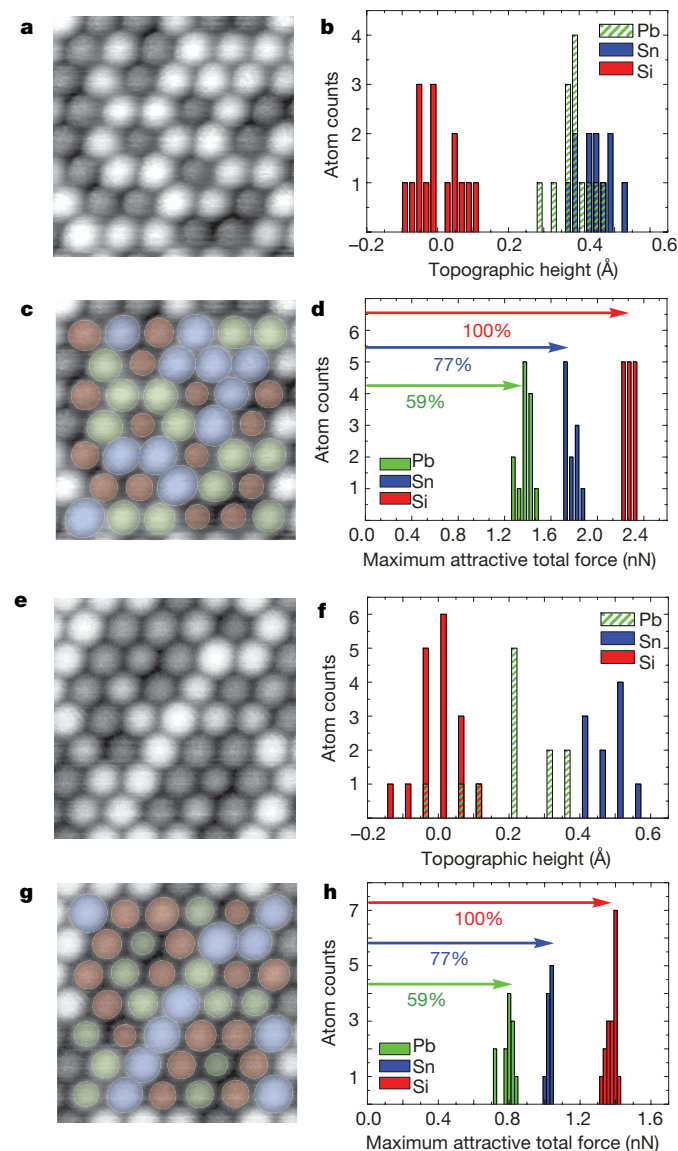


Figure 3 | Single-atom chemical identification. **a**, Topographic image of a surface alloy composed by Si, Sn and Pb atoms blended in equal proportions on a Si(111) substrate. **b**, Height distribution of the atoms in **a**, showing that Pb and Sn atoms with few nearest-neighbouring Si atoms appear indistinguishable in topography. **c**, Local chemical composition of the image in **a**. Blue, green, and red atoms correspond to Sn, Pb and Si, respectively. **d**, Distribution of maximum attractive total forces measured over the atoms in **a**. By using the relative interaction ratio determined for Sn/Si and Pb/Si (Fig. 2b and d), each of the three groups of forces can be attributed to interactions measured over Sn, Pb and Si atoms. **e**, Topographic image similar to that in **a**, but showing a region where some Pb atoms are almost completely surrounded by Si atoms. These Pb atoms (identified in **g** by a darker shade of green) are indistinguishable from the surrounding Si atoms, as illustrated by the topographic height distribution histogram (**f**). The local chemical composition, shown in **g**, can still be unambiguously assigned by measuring the total force values over each surface atom and using the relative interaction ratios for Sn/Si and Pb/Si to attribute the three groups of maximum attractive forces to interactions measured over Sn, Pb and Si atoms (**h**). The colour code for labelling the Pb, Sn and Si atoms in **g** is the same as in **c**. Image dimensions are $(4.3 \times 4.3) \text{ nm}^2$. The images were acquired close to the onset of the short-range interaction²⁰; for the acquisition parameters see the Supplementary Information.

(Fig. 3a and e). In this instance, we systematically recorded the total tip–surface interaction force over each atom seen in the images in Fig. 3a and e, respectively. The measured maximum attractive total forces were found to fall into three distinct groups (see histograms in Fig. 3d and h, respectively). When taking into account the relative interaction ratio for Sn and Si and for Pb and Si determined in our earlier experiments (Fig. 2b and d), these groups can be assigned to forces obtained over Sn, Pb and Si atoms (Fig. 3d and h) and hence the chemical identity of each surface atom can be determined (Fig. 3c and g). The significant discrepancy between the total force values in Fig. 3d and h—obtained in two separate measurement sessions using different tips—confirms that although tip characteristics strongly influence measured forces, they do not affect the ability to chemically identify surface atoms. These results also corroborate the robustness of the procedure, as the identification in Fig. 3 has been accomplished by using the maximum attractive total forces instead of the short-range forces. This more straightforward identification process, which avoids the non-trivial and time-consuming separation of the short- and long-range contributions to the total force²⁰, can be extended to other systems if the total force is not dominated by long-range interactions and there are no pronounced in-plane local spatial variations of the long-range forces. In the experiments shown in Fig. 3, for instance, the long-range contribution at the minimum positions was only 10% to 18% of the total interaction force (see the Supplementary Information).

We note that it would have been impossible to reveal the local atomic composition of these surface alloy regions using topographic information. For example, in areas with locally homogeneous distributions of Si atoms (Fig. 3a), Pb and Sn appear indistinguishable in topography; this is clearly illustrated by the atomic height distribution histogram (Fig. 3b). But in regions where Si atoms cluster together (Fig. 3e), any Pb atoms that are surrounded almost completely by Si atoms (differentiated from other Pb atoms in Fig. 3g by a darker shade of green) are indistinguishable from the Si atoms; again, this effect is clearly illustrated by the histogram shown in Fig. 3f. These topographic variations with the number of nearest-neighbouring Si atoms^{20,21} have been attributed to a subtle coupling between charge transfer and atomic relaxations²². For closer tip–surface distances, relative variations in the atomic contrast—which would further hinder a topographic discrimination attempt—are expected owing to differences in the strength of the interaction forces over the atoms and tip-induced atomic relaxations²⁰. Attempts to scan at tip–surface distances close to the maximum attractive forces—where the interaction between the outermost tip atom and a surface atom dominates the signal, and hence unambiguous chemical information of the atomic surface species can be obtained—result in most of the cases in unstable imaging, or even in modifications of the tip apex or surface due to strong tip–surface lateral forces.

The present approach to characterizing the local composition of a multi-element system at the atomic level, which is based on the detection of the short-range chemical forces between the outermost atom of an AFM tip and individual surface atoms, should be widely applicable. It does require prior calibration of the relative interaction ratio of the maximum attractive short-range forces between pairs of atomic species on a well-defined system; but once obtained, the ratios (which are practically independent of tip apex characteristics) can serve as fingerprints for chemical recognition in subsequent measurements. We believe that the chemical identification capabilities demonstrated here hold substantial promise for affecting research areas such as catalysis, materials science or semiconductor technology, in which important functional properties are controlled by the chemical nature and short-range ordering of individual atoms, defects, adsorbates or dopants.

METHODS

Dynamic force microscopy and spectroscopy measurements. We used a home-built ultrahigh vacuum dynamic AFM powered by a commercial scanning probe controller (Dulcinea, Nanotec Electrónica, Madrid, Spain) and operated at room

temperature under the frequency modulation detection method²³. The cantilever was instantaneously excited to its first mechanical resonant frequency keeping the oscillation amplitude constant. The main observable was the shift of the first mechanical resonant frequency (Δf) from the free-oscillation value upon the forces acting on the tip at the cantilever free end²⁴. Force spectroscopy was performed recording the Δf signal as a function of the tip-sample relative vertical displacement (Z). The determination of the corresponding cantilever stiffness and oscillation amplitude values is described elsewhere¹². The absence of any tip or surface modification during the spectroscopic acquisition was carefully and properly checked¹². During imaging, and for each spectroscopic measurement, the long-range electrostatic interaction was minimized by compensating the tip-surface contact potential difference. For the calibration of the relative interaction ratio in Fig. 2, we first performed the identification of Sn, Pb, and Si in the corresponding bi-atomic overlayers (Fig. 1d, e) by changing the relative concentration of the two elements²⁰.

In Fig. 2, a single spectroscopic measurement comprised the successive acquisition of a hundred equivalent $\Delta f(Z)$ curves over the topmost part of the surface atom with a lateral precision better than $\pm 0.1 \text{ \AA}$, provided by our atom-tracking implementation^{12,16}. In each case, these $\Delta f(Z)$ curves were averaged in a single $\Delta f(Z)$ characteristic from which we obtained the total interaction force using the inversion procedure proposed by Sader and Jarvis²⁵. For each set of curves, the compensation of the topographic effects on Z associated with the spectroscopic acquisition²⁰ was then undertaken; this sets the separation distance between the two force minima and provides a common origin with respect to the surface plane²⁰. The short-range chemical forces were obtained afterwards by the subtraction of an appropriate fit^{11,12} over the long-range interaction region to the total force, where this long-range region is defined from the free oscillation to the Z position at which both curves start splitting owing to the onset of the short-range interaction. For clarity in the representation, the origin of the Z axis for each set was shifted to the position for the Si minimum (keeping the original separation between the minima constant), so that all the sets share the same distance origin when compared. In the case of the experiments shown in Fig. 3, only ten $\Delta f(Z)$ curves were measured over each atom. The surface alloy was prepared by the deposition of approximately one-sixth of a monolayer of Pb—one monolayer corresponds to the surface atomic density of a (111) plane of a Si crystal—and one-ninth of a monolayer of Sn over the Si(111)-(7 × 7) surface, followed by sample annealing at 700 K.

First-principles calculations. Calculations are based in density functional theory implemented with a local orbital basis using the FIREBALL code²⁶, which offers a very favourable accuracy-to-efficiency balance. The details of the minimal basis we used are described elsewhere²⁰. To model the surface we considered a (6 × 6) periodic slab that includes six Si layers with H saturating the dangling bonds at the deeper layer (Fig. 1b). Only the Γ point was included in the sampling of the Brillouin zone. The tip-surface interaction energy was determined in a stepwise, quasistatic manner by approaching the tip parallel to the surface. At each step, the atoms in the slab and the tip model were allowed to relax to their ground-state configuration with convergence criteria for the total energy and forces of 10^{-6} eV and 0.05 eV \AA^{-1} . Only the H-saturated atoms at the topmost part of the tip models (Fig. 2e and f) and the Si and H layers at the bottom of the slab were fixed during the relaxation process. The short-range forces were calculated as a numerical derivative of the total energy.

Received 12 August; accepted 4 December 2006.

- Eigler, D. M. & Schweizer, E. K. Positioning single atoms with a scanning tunnelling microscope. *Nature* **344**, 524–526 (1990).
- Sugimoto, Y. *et al.* Atom inlays performed at room temperature using atomic force microscopy. *Nature Mater.* **4**, 156–159 (2005).
- Stipe, B. C., Rezaei, M. A. & Ho, W. Single-molecule vibrational spectroscopy and microscopy. *Science* **280**, 1732–1735 (1998).
- Heinrich, A. J., Lutz, C. P., Gupta, J. A. & Eigler, D. M. Molecule cascades. *Science* **298**, 1381–1387 (2002).

- Pascual, J. I., Lorente, N., Song, Z., Conrad, H. & Rust, H.-P. Selectivity in vibrationally mediated single-molecule chemistry. *Nature* **423**, 525–528 (2003).
- Madhavan, V., Chen, W., Jamneala, T., Crommie, M. F. & Wingreen, N. S. Tunneling into a single magnetic atom: spectroscopic evidence of the Kondo resonance. *Science* **280**, 567–569 (1998).
- Li, J., Schneider, W.-D., Berndt, R. & Delley, B. Kondo scattering observed at a single magnetic impurity. *Phys. Rev. Lett.* **80**, 2893–2896 (1998).
- Morita, S., Wiesendanger, R. & Meyer, E. *Noncontact Atomic Force Microscopy*. *NanoScience and Technology* (Springer, Berlin, 2002).
- García, R. & Pérez, R. Dynamic atomic force microscopy methods. *Surf. Sci. Rep.* **47**, 197–301 (2002).
- Giessibl, F. J. Advances in atomic force microscopy. *Rev. Mod. Phys.* **75**, 949–983 (2003).
- Lantz, M. A. *et al.* Quantitative measurement of short-range chemical bonding forces. *Science* **291**, 2580–2583 (2001).
- Abe, M., Sugimoto, Y., Custance, O. & Morita, S. Room-temperature reproducible spatial force spectroscopy using atom-tracking technique. *Appl. Phys. Lett.* **87**, 173503 (2005).
- Hoffmann, R., Kantorovich, L. N., Baratoff, A., Hug, H. J. & Güntherodt, H.-J. Sublattice identification in scanning force microscopy on alkali halide surfaces. *Phys. Rev. Lett.* **92**, 146103 (2004).
- Pérez, R., Payne, M., Stich, I. & Terakura, K. Role of covalent tip-surface interactions in noncontact atomic force microscopy. *Phys. Rev. Lett.* **78**, 678–681 (1997).
- Livshits, A. I., Shluger, A. L., Rohl, A. L. & Foster, A. S. Model of noncontact scanning force microscopy on ionic surfaces. *Phys. Rev. B* **59**, 2436–2448 (1999).
- Abe, M., Sugimoto, Y., Custance, O. & Morita, S. Atom tracking for reproducible force spectroscopy at room temperature with non-contact atomic force microscopy. *Nanotechnology* **16**, 3029–3034 (2005).
- Oyabu, N. *et al.* Single atomic contact adhesion and dissipation in dynamic force microscopy. *Phys. Rev. Lett.* **96**, 106101 (2006).
- Ke, S. H., Uda, T., Pérez, R., Stich, I. & Terakura, K. First-principles investigation of tip-surface interaction on a GaAs(110) surface: implications for atomic force and scanning tunneling microscopies. *Phys. Rev. B* **60**, 11631–11638 (1999).
- Hembacher, S., Giessibl, F. J. & Mannhart, J. Force microscopy with light-atom probes. *Science* **305**, 380–383 (2004).
- Sugimoto, Y. *et al.* Real topography, atomic relaxations, and short-range chemical interactions in atomic force microscopy: The case of the α -Sn/Si(111)-(√3 × √3)R30° surface. *Phys. Rev. B* **73**, 205329 (2006).
- Sugimoto, Y. *et al.* Non-contact atomic force microscopy study of the Sn/Si(111) mosaic phase. *Appl. Surf. Sci.* **241**, 23–27 (2005).
- Charrier, A. *et al.* Contrasted electronic properties of Sn-adatom-based (√3 × √3)R30° reconstructions on Si(111). *Phys. Rev. B* **64**, 115407 (2001).
- Albrecht, T. R., Grütter, P., Horne, D. & Rugar, D. Frequency modulation detection using high-Q cantilevers for enhanced force microscope sensitivity. *J. Appl. Phys.* **69**, 668–673 (1991).
- Giessibl, F. J. Forces and frequency shifts in atomic resolution dynamic-force microscopy. *Phys. Rev. B* **56**, 16010–16015 (1997).
- Sader, J. E. & Jarvis, S. P. Accurate formulas for interaction force and energy in frequency modulation force spectroscopy. *Appl. Phys. Lett.* **84**, 1801–1803 (2004).
- Jelinek, P., Wang, H., Lewis, J. P., Sankey, O. F. & Ortega, J. Multicenter approach to the exchange-correlation interactions in ab initio tight-binding methods. *Phys. Rev. B* **71**, 235101 (2005).

Supplementary Information is linked to the online version of the paper at www.nature.com/nature.

Acknowledgements We thank F. J. Giessibl and M. Reichling for their comments on the manuscript, and T. Namikawa and K. Mizuta for technical assistance. This work was supported by the Handai FRC, the JST, the 21st Century COE programme, and the MEXT of Japan. The work of P.P. and R.P. is supported by the MCYT, the Juan de la Cierva Programme, the CCC-UAM (Spain), and the FORCETOOL project (EU). The work of P.J. is supported by the MSMT and GAAV.

Author Information Reprints and permissions information is available at www.nature.com/reprints. The authors declare no competing financial interests. Correspondence and requests for materials should be addressed to O.C. (oscar@afm.eei.eng.osaka-u.ac.jp).

Chemical identification of individual surface atoms by atomic force microscopy (Supplementary Information)

Yoshiaki Sugimoto,¹ Pablo Pou,² Masayuki Abe,^{1,3} Pavel Jelinek,⁴ Rubén Pérez,² Seizo Morita,¹ and Óscar Custance^{1,*}

¹Graduate School of Engineering, Osaka University,
2-1 Yamada-Oka, 565-0871 Suita, Osaka, Japan

²Departamento de Física Teórica de la Materia Condensada,
Universidad Autónoma de Madrid, 28049 Madrid, Spain

³PRESTO, Japan Science and Technology Agency, Saitama 332-0012, Japan

⁴Institute of Physics, Academy of Sciences of the Czech Republic,
Cukrovarnicka 10, 1862 53, Prague, Czech Republic

I. AVERAGE RELATIVE INTERACTION RATIO FOR INDIUM AND SILICON

Figure SI-1 presents similar dynamic force spectroscopic measurements to the ones displayed in Fig. 2 yet in another surface of very different chemical properties: a single atomic overlayer of In grown on a Si(111) substrate. As in the Sn and Pb cases (Fig. 1), a small concentration of Si defects with a diminished topographic contrast is also found in this In surface (see the inset image in Fig. SI-1b) that can be identified by changing the relative concentration of In. The sets of short-range (SR) force curves shown in Fig. SI-1a were obtained using the same acquisition and analysis protocols as the ones in Figs. 2a and 2c. For each SR force curve a hundred of frequency shift vs. tip-sample relative vertical displacement $[\Delta f(Z)]$ characteristics were measured over the top-most part of the corresponding atom with a lateral precision better than $\pm 0.1 \text{ \AA}$ (Ref. 1, 2). The sets of SR force curves displayed in Fig. SI-1 were measured over In and Si atoms in an equivalent local surface configuration as the ones pointed in the inset image, but they were collected over multiple measurement sessions involving different tip-apex terminations. As in the case of the Sn and Pb overlayers, unlike force characteristics were registered for different tip apexes. Again, the normalization of the two curves within each set to the absolute value of the minimum SR force for the corresponding Si curve (Fig. SI-1b) reveals the relative interaction ratio of the maximum attractive SR forces for the In and Si system, providing an average value of 0.72 ± 0.04 .

II. ACQUISITION PARAMETERS

Table I summarises the measured values of the cantilever free-oscillation first mechanical resonant frequency (f_0), oscillation amplitude (A), and stiffness (K) at which all the sets of SR force curves shown in this work were acquired. Notice that some sets within each system (Sn-Si, Pb-Si and In-Si) were obtained with the same cantilever under identical acquisition parameters. In those cases, the tip-apex structure was intentionally modified by slight and well controlled tip-surface contacts until obtaining a tip apex stable enough to perform the spectroscopic acquisition without any tip change during the whole process.

Table II summarises the parameters at which the images were acquired. Apart from the cantilever related magnitudes, the values for the frequency shift (Δf) topographic set point are also indicated. The values of f_0 , A and K at which the force curves in the identification experiments shown in Fig. 3 were acquired are the same as for the corresponding images.

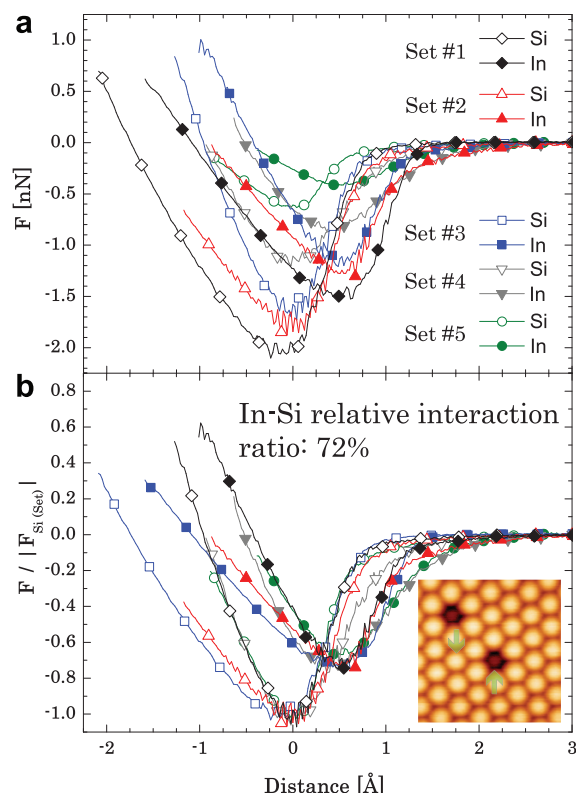


FIG. 1: Measured chemical forces and average relative interaction ratio of the maximum attractive short-range forces for In and Si. As in Fig. 2, each force characteristic was obtained from the measurement of a hundred spectroscopic curves, and the horizontal axis denotes the tip-sample relative vertical displacement distance (see the Methods section in the Letter for details).

III. INDEPENDENCE FROM THE TIP-APEX CHEMICAL TERMINATION

As it has been stated in Sec. II, in the course of the experiments slight tip-surface contacts were produced to intentionally change the tip-apex structure. Thus, it is very likely that the tip-apex chemical termination for some of the sets of force curves measured over the Sn, Pb, and In overlayers differs from Si; the material the tip was originally made from. But when performing the normalization (Figs. 2b and 2d, and Fig. SI-1b), surprisingly, the SR force curves respectively meet at the minima independently from the chemical termination of the tip apex. Furthermore, this feature has been also reproduced by the first-principles calculations on the

TABLE I: Acquisition parameters [free-oscillation first mechanical resonant frequency (f_0), oscillation amplitude (A), and cantilever stiffness (K)] for the sets of SR force curves displayed in Fig. 2 and Fig. SI-1.

Sn-Si	f_0 [Hz]	A [Å]	K [N/m]
Set # 1	193726	255	48.8
Set # 2	193726	255	48.8
Set # 3	162286	259	28.7
Set # 4	162300	219	28.7
Set # 5	162317	253	28.7
Pb-Si	f_0 [Hz]	A [Å]	K [N/m]
Set # 1	160338	277	28.4
Set # 2	160338	277	28.4
Set # 3	154055	224	25.2
Set # 4	154055	224	25.2
Set # 5	154055	224	25.2
In-Si	f_0 [Hz]	A [Å]	K [N/m]
Set # 1	168593	333	32.2
Set # 2	162274	213	31.6
Set # 3	152992	230	26.5
Set # 4	161709	106	31.3
Set # 5	161709	106	31.3

TABLE II: Acquisition parameters [frequency shift set point (Δf), free-oscillation first mechanical resonant frequency (f_0), oscillation amplitude (A) and cantilever stiffness (K)] for the topographic images shown in Figs. 1 and 3, and Fig. SI-1.

Image	Δf [Hz]	f_0 [Hz]	A [Å]	K [N/m]
Fig. 1d	-6.6	162282	253	31.6
Fig. 1e	-3.0	160340	277	28.4
Fig. 3a	-2.5	153364	240	24.9
Fig. 3e	-5.0	152973	155	24.7
Fig. SI-1	-6.2	161705	106	31.3

Sn-Si system as it is shown in Figs. 2e and 2f.

The nearly independent behavior of the relative interaction ratio from the tip-apex chemical termination shown by both experiments and calculations should rely on some basic properties of the chemical bond of these systems that are highlighted by the curves' normalization. To provide a rigorous proof on the general validity of the independence of the relative interaction ratio, which basically allows the chemical identification of individual atoms at the surface, is a rather difficult task due to the complex behavior of the tip-surface interaction. Nevertheless, we explore here a simple, basic explanation in order to gain insight into this certainly far from intuitive result.

In our current understanding of dynamic force microscopy (DFM) imaging on semiconducting surfaces, the atomic contrast is dominated by covalent bonding interactions between a dangling bond pointing out of the tip-apex atom and the dangling bonds at the surface atoms. These surface dangling bonds associated with the different chemical constituents are not individual entities, but, on the contrary, due to the multiple interactions associated with the translational periodicity of the surface, they combine to form extended states that ultimately control the chemistry of the system. When probing the surface in the weak attractive interaction regime (like dynamic force microscopy does under normal imaging conditions), the surface structure is almost unperturbed, and the

strength of the tip-surface chemical interaction is still controlled by the character of the extended surface states. On the contrary, around the tip-surface distance that corresponds to the maximum attractive SR force, the calculations show that the surface structure significantly distorts³ in order to accommodate an atomic distance between the tip-apex outermost atom and the surface atom that is close to the sum of the corresponding covalent radii, revealing that the dominant contribution to the interaction comes from the bonding between those two atoms.

Thus, probing near the maximum attractive force highlights the intrinsic contribution of the tip-apex-surface-atom dimer, and we can expect some basic properties of the bonding of diatomic molecules to hold⁴. This dimer interaction could be roughly associated with the bond stretching (or pair-wise) term that is used as the fundamental energetic contribution in many approximate descriptions of the atomic bonding (based either in classical potentials or parameterized quantum LCAO calculations). One of the properties of the bond stretching, concerning the bond energetics, states that the heterogeneous covalent interaction between a pair of elements t and α , can be approximated as the geometric mean of the homogeneous interaction of the corresponding elements, $t-t$ and $\alpha-\alpha$, i.e., $E_{t-\alpha}^0 \approx \sqrt{E_{t-t}^0 \times E_{\alpha-\alpha}^0}$ (see, for example, Ref. 4). According to the bond stretching properties, the maximum attractive force $F_{t-\alpha, \max}$ should be proportional to the dissociation energy $E_{t-\alpha}^0$ divided by a characteristic decay length $R_{t-\alpha}^*$ of the interaction, i.e. $F_{t-\alpha, \max} \propto E_{t-\alpha}^0 / R_{t-\alpha}^*$. It is not obvious that the combination rule for $R_{t-\alpha}^*$ can be correctly defined in terms of a geometric mean relation $R_{t-\alpha}^* \approx \sqrt{R_{t-t}^* \times R_{\alpha-\alpha}^*}$, which would yield directly the constant value of the relative interaction ratio. However, if the differences between $R_{\alpha-\alpha}^*$ and R_{t-t}^* are small enough, which is certainly the case for the atoms (Si, Sn, Pb, In) considered here, this approximation is justified.

Therefore, these *phenomenological* combination rules provide a natural explanation for the relative bonding strengths revealed by the normalization procedure.

Following the arguments presented above, the relative interaction ratio can be applied to identify atoms in a multi-element semiconductor system. For a given tip-apex of unknown chemical termination, when individually probing the different atoms of such system close to the maximum attractive force, interactions dominated by the bond between the different pairs of atomic species are obtained. Considering the interaction at the SR force minima of the tip-apex outermost atom (t) with two separate atoms (α and β) of this multi-element system ($F_{t-\alpha, \max}$ and $F_{t-\beta, \max}$, respectively), under the above stated condition for the relative decay length term, the relative interaction ratio would then satisfy the relation:

$$\frac{F_{t-\alpha, \max}}{F_{t-\beta, \max}} \approx \frac{\sqrt{F_{t-t, \max} \times F_{\alpha-\alpha, \max}}}{\sqrt{F_{t-t, \max} \times F_{\beta-\beta, \max}}} \approx \sqrt{\frac{F_{\alpha-\alpha, \max}}{F_{\beta-\beta, \max}}} \quad (1)$$

where $F_{t-t, \max}$, $F_{\alpha-\alpha, \max}$ and $F_{\beta-\beta, \max}$ denote the homogeneous interaction of the corresponding elements at the SR force minima. Absolute deviations from the geometric mean, however, are reflected in the broadening of the histogram peaks of the relative interaction ratio. Thus, when taking the relative interaction ratio, the common features associated with the structural characteristics of the tip-apex cancel out—as stated in the text—and, additionally, the influence of the chemical nature of the tip-apex outermost atom is minimized.

This assumption has been further supported by first-principles calculations using the two tip-apex structures shown in Fig. 2 considering all the possible chemical terminations among the elements involved in the identification experiments of Fig. 3 (Sn, Pb and Si). The structure shared by Tip 1 and Tip 2 (Tip B in the following) was respectively terminated in a Sn, a Pb, and a Si atom, and these three different terminated tips were used to probe three finite clusters with a Sn, a Si, and a Pb atoms, respectively, in a similar adsorption structure to the one they present at the surface.

TABLE III: Calculated relative interaction ratios for three chemical terminations of the tip-models shown in Fig. 2.

Tip B	Surface atom			Tip A	Surface atom		
	Si	Sn	Pb		Si	Sn	Pb
Si	100%	82%	67%	Si	100%	78%	62%
Sn	100%	84%	68%	Sn	100%	79%	59%
Pb	100%	82%	64%	Pb	100%	71%	54%

The same strategy was adopted for the structure shared by Tip 3 and Tip 4 (Tip A in the following). The simplified model for the surface—that preserves the local coordination with the four relevant nearest neighbours and provides the correct hybridisation for the surface atom states—was imposed by the large computational resources required for a calculation of the 18 different force-versus-distance curves taking into account the full surface periodicity. The small size of the surface cluster—the corresponding surface atom, 9 Si atoms plus the corresponding saturating hydrogen atoms—precludes the inclusion of relaxations during the calculation of the SR forces. The resulting relative interaction ratio of the maximum attractive force values, referred to the surface Si atom, are summarised in Table III. Independently from the identity of the atom at the tip-apex end, these ratios resemble the ones obtained experimentally and their average values (79% for Sn and 62% for Pb) are quite close to the experimental ones. The slight variations between the values obtained with the Tip A and the Tip B might concern more the unlike hybridisation state of the atom at the end of Tip B together with the importance of the atomic relaxations in that tip⁵ (not included in the present calculations) than to the different tip-apex chemical termination.

In view of all of these evidences, the relative maximum attractive interaction ratio provides the basis for the formulation of a protocol for single-atom chemical identification in multi-element systems under a certain covalent component in the tip-surface interaction. The identification procedure requires first the calibration of the relative interaction ratio between the pairs of atomic species involved with respect to one of them—typically the one providing the stronger SR interaction force—on a well-defined system as the bi-atomic surfaces shown in Figs. 1d and 1e, and Fig. SI-1. The precise characterization of the maximum attractive SR interaction force over each atom will allow then to discriminate between the different atomic species at the multi-element system. Upon enough precision in both the detection of these SR chemical forces and the ratios' calibration, the tabulated values of the relative interaction ratio of the maximum attractive SR force values can then be used for the unambiguous identification of the atomic species as shown in Fig. 3.

A final remark on the generality of this single-atom chemical identification protocol is due. The arguments presented above provide an explanation for the observed behavior of the relative interaction ratio in semiconductor surfaces. They certainly required strong approximations on the description of the interaction, but they are justified for these systems in the distance regime close to the maximum attractive SR interaction. We hope that these considerations could stimulate further work leading to a more conclusive proof and the extension of these ideas to other systems where SR forces, although different in nature, also dominate the observed atomic scale contrast.

IV. LONG-RANGE INTERACTION FORCE CONSIDERATIONS

As it has been discussed within the text, the use of the total force instead of the SR chemical interaction for the identification of single atoms through the comparison with the tabulated relative

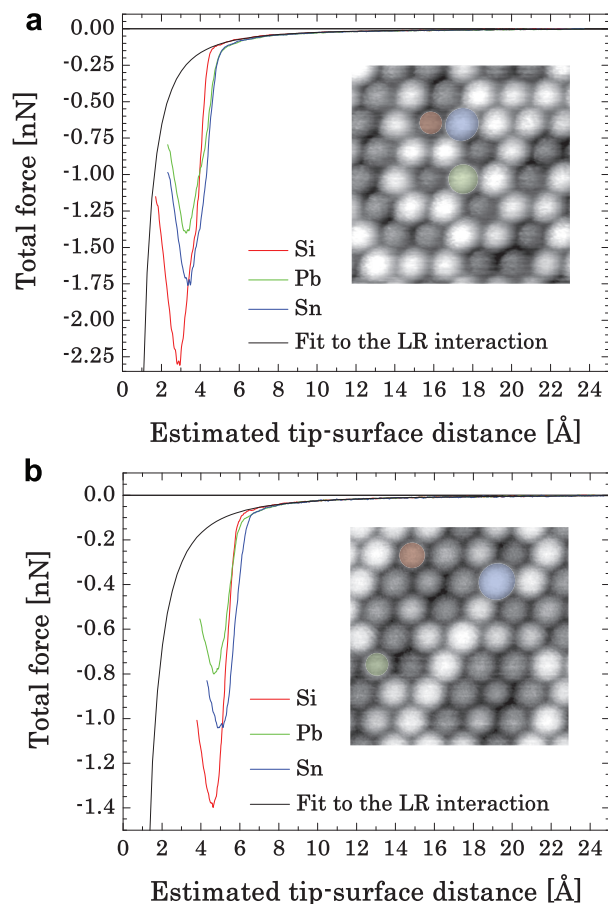


FIG. 2: Total force curves extracted from the experiments shown in Fig. 3 together with the estimation of the LR forces (black lines) from fits to the total force over the LR interaction region, i.e. from the free oscillation region to the onset of the SR chemical forces. **a**, These three force curves were acquired, respectively, over the Si (red), Sn (blue) and Pb (green) atoms highlighted in the inset image, which corresponds with the topography shown in Fig. 3a. **b**, Similar set of total force curves measured over the highlighted atoms in the inset, which corresponds with the topographic image in Fig. 3e; the colour code for curves and atoms is the same as in **a**. Note that the three force curves within each set (**a** and **b**) share almost the same behaviour over the LR interaction region, pointing towards a nearly common origin with respect to the surface plane³.

interaction ratio is conditioned to the presence of a very small, and spatially homogeneous, contribution of the long-range (LR) interaction to the total force. This is the case, for instance, of the experiments shown in Fig. 3.

The magnitude of the LR forces in those experiments, and its dependence with the tip-surface distance, is illustrated in Fig. SI-2, where two sets of three force curves measured, respectively, over a Si (red), a Sn (blue) and a Pb (green) atom are displayed. One set (Fig. SI-2a) corresponds to the experiment shown in Figs. 3a to 3d, while the other (Fig. SI-2b) was taken from the experiment summarized in Figs. 3e to 3h. To estimate the LR contribution to the total force in these sets, we have performed the same analysis carried out for the separation of the SR chemical interaction from the total force in the experiments reported in Fig. 2. First, for each set of force curves, the compensation of the topographic effects on Z originated by the acquisition using the atom-tracking technique³ was undertaken; this settles the separation distance between the force minima and approximately provides a common distance origin with respect to the surface plane, so that the curves share the same LR interaction³ (Fig. SI-2). In Fig. 2, the SR chemical forces

TABLE IV: Summary of the relative strength (R) of the estimated LR interaction force at the total force minimum positions (F_{LR}) with respect to the registered maximum attractive force values (F_{Min}) in the curves shown in Figs. SI-2a (Si^a , Sn^a , and Pb^a) and SI-2b (Si^b , Sn^b , and Pb^b), respectively.

Atom	F_{Min} [nN]	F_{LR} [nN]	R [%]
Si^a	-2.30	-0.32	14
Sn^a	-1.75	-0.23	13
Pb^a	-1.40	-0.25	18
Si^b	-1.39	-0.13	9
Sn^b	-1.03	-0.12	12
Pb^b	-0.80	-0.11	14

were obtained afterwards by the subtraction of an appropriate fit^{1,6} to the total force over the LR interaction region, where this region is defined from the free oscillation —complete absence of interaction force— to the Z position at which the curves start splitting due to the onset of the SR interaction. These analytical fits are displayed in Fig. SI-2, and the corresponding force values are summarized in Table IV. From them, it can be seen that the LR contribution to the total force value at the minimum positions in the identification experiment of Figs. 3a to 3d was between a 14% to a 18%; and in the experiment of Figs. 3e to 3h, it was only between a 9% to a 14%. Besides, this LR contribution over Si atoms is slightly larger than over the other atoms. Therefore, this small contribution of the LR interaction at the total force minima enables the direct comparison of the total force minimum values (Figs. 3d and 3h) with the tabulated relative interaction ratios of the maximum attractive SR forces shown in Fig. 2.

One of the LR forces to take into account for single-atom chemical identification using DFM is the electrostatic interaction. In the experiments presented in this work, the LR electrostatic interaction was minimized during imaging, and for each spectroscopic measurement, by compensating the tip-surface contact potential difference (CPD). The CPD measurement was carried out by swapping the bias voltage between tip and sample while recording the frequency shift $[\Delta f(V)]$ at a tip-surface distance slightly above the onset of the SR chemical interaction. Since in our experiments both tip and sample were highly conductive, small CPD values were usually obtained; for instance, the CPD values for the experiments shown in Figs. 3a to 3d and Figs. 3e to 3h were -189 mV and 76 mV, respectively. Since the CPD was measured close enough to the surface, its values were quite small, and, additionally, they were further compensated, the LR contribution to the total force within the range we probed the SR chemical forces mainly comes from the van der Waals interaction. This is consistent with the estimations we obtain from the LR fits⁶ regarding the surface plane position and the tip radius, with values for the latter (4 to 6 nm) smaller than the nominal radius provided by the cantilevers' manufacturer. The origin of the distance axes in Fig. SI-2 corresponds to the surface plane position, roughly estimated as the divergence of the LR fit³.

The weak LR force conditions above mentioned favour the use of the total interaction force for single-atom chemical identification. Note, however, that upon a stronger, or spatially inhomogeneous, contribution of the LR interaction to the total force, the here presented identification method is still applicable. In these cases, the identification relies on measuring the total forces over the atoms and obtaining, afterwards, the SR forces following a similar separation procedure to the one discussed for the sets of curves shown in Fig. 2, or another alternative method⁷.

* Corresponding author:

oscar@afm.eei.eng.osaka-u.ac.jp

- ¹ Abe, M., Sugimoto, Y., Custance, O. & Morita, S. Room-temperature reproducible spatial force spectroscopy using atom-tracking technique. *Appl. Phys. Lett.* **87**, 173503 (2005).
- ² Abe, M., Sugimoto, Y., Custance, O. & Morita, S. Atom tracking for reproducible force spectroscopy at room temperature with non-contact atomic force microscopy. *Nanotechnology* **16**, 3029–3034 (2005).
- ³ Sugimoto, Y., Pou, P., Custance, O., Jelinek, P., Morita, S., Pérez, R. & Abe, M. Real topography, atomic relaxations, and short-range chemical interactions in atomic force microscopy: The case of the $\alpha\text{-Sn/Si}(111)-(\sqrt{3} \times \sqrt{3})R30^\circ$ surface. *Phys. Rev. B* **73**, 205329 (2006).

- ⁴ Pauling, L. *The nature of the chemical bond* (Cornell University Press, Ithaca, New York, 1960), 3rd, 13th printing 1995 edn.
- ⁵ Oyabu, N., Pou, P., Sugimoto, Y., Jelinek, P., Abe, M., Morita, S., Pérez, R. & Custance, O., Single atomic contact adhesion and dissipation in dynamic force microscopy. *Phys. Rev. Lett.* **96**, 106101 (2006).
- ⁶ Lantz, M. A. *et al.* Quantitative measurement of short-range chemical bonding forces. *Science* **291**, 2580–2583 (2001).
- ⁷ Hoffmann, R., Kantorovich, L. N., Baratoff, A., Hug, H. J. & Güntherodt, H.-J. Sublattice identification in scanning force microscopy on alkali halide surfaces. *Phys. Rev. Lett.* **92**, 146103 (2004).



50 YEARS AGO

In an article on "Nuclear Knowledge and Christian Responsibility" in the *London Quarterly* for January 1957, Prof. C. A. Coulson emphasizes that if the under-developed countries are also to enjoy the benefits of civilization, or indeed if our civilization is to continue, a fair and reasonable distribution of nuclear energy is an absolute necessity... he argues that it is a Christian responsibility to see that nuclear energy, like any other scientific discovery, is rightly used... Urging that we should be profoundly grateful for our nuclear knowledge, Prof. Coulson indicates some of the ways in which we should share and develop nuclear energy and its applications... We should also rejoice in new possibilities for curing disease and improving health in parts of the world where disease is rampant and health poor and should see that no one makes personal profit out of this situation to the detriment of the world-wide distribution of the new products.

From *Nature* 2 March 1957.

100 YEARS AGO

On Leprosy and Fish Eating. A Statement of Facts and Explanations. By Jonathan Hutchinson — The object of this work is stated in the preface to be "to carry conviction to the reader that the fundamental cause of the malady known as true leprosy is the eating of fish in a state of commencing decomposition."... Mr. Hutchinson would associate the former prevalence of leprosy in the British Isles and in Europe with the Roman Catholic ordinances prescribing fish-food on two out of every three weekdays... We think that Mr. Hutchinson goes much too far in thus ascribing all variations in the prevalence of leprosy as being correlated with those of a fish-diet; even in the fact that the disease is more prevalent among men than among women he sees support for his hypothesis, for he suggests that women are more fastidious feeders than men.

From *Nature* 28 February 1907.

- Sokolov, S., Scheuer, T. & Catterall, W. A. *Neuron* **47**, 183–189 (2005).
- Starace, D. M. & Bezanilla, F. *Nature* **427**, 548–553 (2004).
- Tombola, F., Pathak, M. M., Gorostiza, P. & Isacoff, E. Y. *Nature* **445**, 546–549 (2007).
- Larsson, H. P., Baker, O. S., Dhillon, D. S. & Isacoff, E. Y. *Neuron* **16**, 387–397 (1996).
- Yang, N., George, A. L. Jr & Horn, R. *Neuron* **16**, 113–122 (1996).
- Freites, J. A., Tobias, D. J. & White, S. H. *Biophys. J.* **91**, L90–L92 (2006).
- Ahern, C. A. & Horn, R. *Neuron* **48**, 25–29 (2005).
- Struyk, A. F., Scoggan, K. A., Bulman, D. E. & Cannon, S. C. *J. Neurosci.* **20**, 8610–8617 (2000).
- Cannon, S. C. *Neuromusc. Disord.* **12**, 533–543 (2002).
- Yarov-Yarovoy, V., Baker, D. & Catterall, W. A. *Proc. Natl Acad. Sci. USA* **103**, 7292–7297 (2006).

MICROSCOPY

Atomic fingerprinting

Alexander Shluger and Tom Trevethan

Atomic force microscopy is a well-established technique to image all kinds of surfaces at the atomic scale. But the force patterns that emerge can also pin down the chemical identity of individual atoms.

Picking lentils from ashes is one of the many challenging tasks delegated to fairy-tale characters. In a famous story, Cinderella completes this chore assisted by some helpful doves. Sugimoto *et al.*, in work that appears on page 64 of this issue¹, tackle a similar, but potentially more useful problem: how to identify a particular element on a surface that contains a mixture of elements using only a mechanical probe.

This is, in fact, one of the thorniest problems in surface science. Although the atomic force microscope (AFM) is starting to be used routinely to 'image' surfaces on the atomic scale, interpreting its images is still extremely difficult. The AFM was invented just over 20 years ago, and is now the most widely used scanning probe. Unlike the more mature scanning tunnelling microscope (STM), which can be used only for conducting surfaces, the AFM can image both insulating and conducting samples. But its evolution into a metrology tool capable of discriminating, or even determining, the chemical identities of individual atoms is a new development. It is akin to asking Cinderella to perform her sorting task blindfolded, relying only on the sensation in her fingers.

An AFM works by probing the force acting between its sharp tip and the atoms of the sample's surface. Over the past decade, there have been many spectacular achievements in the imaging and even manipulation of surface structures and individual atoms using an AFM in its dynamic or 'non-contact' mode^{2–5}. In this mode, the AFM's tip is attached to the end of a flexible cantilever, which is oscillated at its resonant frequency and with constant amplitude in a direction perpendicular to the sample surface.

As the tip vibrates, it interacts with the sample's surface, causing the resonant frequency of its oscillations to change. These variations can be measured precisely as a function of tip position, and converted into a three-dimensional image of the surface that contains details at the atomic scale. But relating even simple image patterns to the position of surface atoms and

their chemical identities is a tricky task. The imaging mechanism is complex, and, crucially, the exact composition of the tip's apex on the atomic scale — and so its contribution to the strength of the interaction — is impossible to establish with certainty^{2,4}.

So how does one sort the lentils from the ashes — or, less figuratively, tell apart atoms such as silicon (Si), tin (Sn) and lead (Pb) — using such a method? Sugimoto *et al.*¹ first looked at whether Sn and Pb atoms adsorbed on a silicon surface could be distinguished from each other by correlating topographic AFM images with the adsorbates' known concentrations. To create a transferable mechanistic 'sensation' of these atoms, they then measured with very high accuracy the dependence of the force on the distance between the AFM's tip and the individual atoms on the surface, in a similar way to previous studies^{6,7}.

After repeating their measurements many times, the authors realized that the forces measured above Si, Sn or Pb atoms vary from experiment to experiment. That is most probably because the shape and composition of the tip apex on the atomic scale differed between experiments. If the tip's structure were impossible to determine or control, and the experiments were to be deemed irreproducible, then the whole exercise would be ruined.

Trying to identify a characteristic that would allow force curves measured with different tip terminations to be compared, the authors noticed that the strongest interaction was always between the tip and Si atoms on the surface. So they divided the maximum attractive forces for Sn and Pb adsorbates by the maximum force measured with the surface Si atoms. In this way, they managed to obtain what seemed to be distinct, reproducible force 'fingerprints' for each different type of atom.

How can one be sure that the subtle differences between the force fingerprints are in fact due to the different chemical identities of the atoms? To understand and support their findings, the authors used atomistic modelling¹ to determine plausible atomic structures for the

tip, and used these structures to calculate the forces. This sort of realistic theoretical modelling of the interaction between the tip and the surface, and even of the entire experimental procedure, has become an integral and essential component of many AFM experiments^{4,7}. The results of Sugimoto and colleagues' simulations matched well with those of their experiments. With increased confidence in their fingerprinting technique, the authors prepared an alloy of Si, Sn and Pb atoms on the silicon surface. By measuring the dependence of the force on the distance between the AFM's tip and individual surface atoms, and comparing it with the atomic fingerprints, they could label all atoms

in the image with their chemical identity.

Sugimoto and colleagues' work marks an important step in establishing the AFM as a metrology tool on the atomic scale. It demonstrates that, as is possible with tunnelling current and scanning tunnelling microscopy⁸, a statistical approach to measuring force can provide the local composition and structure of a semiconductor surface at the atomic level. Their findings will inspire similar studies of more complex, truly insulating surfaces, and stimulate further development of such extremely discriminatory chemical analyses.

Alexander Shluger and Tom Trevethan are in the London Centre for Nanotechnology and

the Department of Physics and Astronomy, University College London, Gower Street, London WC1E 6BT, UK.
e-mail: a.shluger@ucl.ac.uk

1. Sugimoto, Y. *et al. Nature* **446**, 64–67 (2007).
2. Morita, S., Wiesendanger, R. & Meyer, E. (eds) *Non-Contact Atomic Force Microscopy* (Springer, New York, 2002).
3. Giessibl, F. J. *Rev. Mod. Phys.* **75**, 949–983 (2003).
4. Foster, A. S. & Hofer, W. *Scanning Probe Microscopes: Atomic Scale Engineering by Forces and Currents* (Springer, New York, 2006).
5. Sugimoto, Y. *et al. Nature Mater.* **4**, 156–159 (2005).
6. Lantz, M. A. *et al. Science* **291**, 2580–2583 (2001).
7. Hoffmann, R., Kantorovich, L. N., Baratoff, A., Hug, H. J. & Güntherodt, H.-J. *Phys. Rev. Lett.* **92**, 146103 (2004).
8. Schmid, M., Stadler, H. & Varga, P. *Phys. Rev. Lett.* **70**, 1441–1444 (1993).

VIROLOGY

Holed up in a natural crystal

Felix A. Rey

Insect viruses that cause polyhedrosis produce infectious microcrystals within a cell. These inclusions were used in a study that pushed the state of the crystallographic art to explain their exceptional stability.

Much of structural biology relies on obtaining highly ordered crystals of proteins and other macromolecules, and it often takes considerable time and effort to produce crystals of adequate quality. In some cases, however, proteins crystallize spontaneously *in vivo*. In such situations the crystals themselves have a biological role (usually storage), examples being insulin¹ and eosinophil major basic protein². Also, the insect polyhedrosis viruses encode a protein called polyhedrin that forms polyhedral crystals, or polyhedra, within an infected cell³. The virus particles, or virions, are protected within these polyhedra and can remain infectious for years outside cells, even in harsh environmental conditions. The polyhedra break down and release the virus only when ingested into the very alkaline environment of the midgut of insect larvae (pH 10–11), resulting in infection of a new host.

Until now, the *in vivo* polyhedra were considered to be too small for single-crystal diffraction experiments. On page 97 of this issue, however, Coulibaly *et al.*⁴ report the use of the latest X-ray diffraction techniques to determine the structure of the polyhedrin protein of silkworm cytoplasmic polyhedrosis virus (CPV) at 2 Å resolution from microcrystals grown *in vivo*. The crystals came from insect cells infected with either wild-type CPV or with a

recombinant baculovirus expressing the CPV polyhedrin gene (Fig. 1a).

Several insect viruses have converged on the strategy of forming polyhedral inclusion bodies to protect themselves and remain infectious for long periods. As well as CPV, which is an RNA virus, baculoviruses such as the nuclear polyhedrosis virus (NPV), and the insect pox viruses (both from families of DNA viruses that are otherwise completely unrelated), use

this strategy³. Described in technical terms, the CPV polyhedra are body-centred-cubic crystals of space group I23. Intriguingly, polyhedra from CPV and NPV, which show no homology detectable by amino-acid sequence similarity, have the same I23 symmetry and identical crystal unit-cell parameters^{5,6}, a coincidence that is hardly fortuitous. So, what's special about the three-dimensional lattice of polyhedra?

Electron micrographs of infectious CPV polyhedra clearly show the virions incorporated within the crystal; they appear as spherical disruptions in an otherwise regular lattice (Fig. 1b). The diameter of CPV particles is about 700 Å (ref. 7), about seven times greater than the unit-cell edge of polyhedra (103.8 Å per side). Each virion incorporated in the crystal thus takes up the space of about 150 unit cells. Several thousand infectious particles are incorporated in an average polyhedron with edges 2 micrometres long, occupying about

10–15% of the total volume of the crystal. Therefore, the polyhedrin packing contacts must be strong enough to make this sort of 'Gruyère' crystal very stable.

Remarkably, Coulibaly *et al.*⁴ found no difference in the diffraction patterns of wild-type infectious polyhedra and those made by recombinant polyhedrin, which have a regular lattice with no virions incorporated. Polyhedrin thus seems to have special packing properties.

Crystals of insulin or eosinophil major basic protein form only within secretory vesicles and dissolve when exposed to the extracellular milieu. Large enough crystals of these two proteins for structural studies could thus be obtained after their isolation and recrystallization under biochemically controlled conditions. In contrast, polyhedrin crystals grow in the cytoplasm (or in the nucleus in the case of NPV) of the infected cell, within a highly heterogeneous

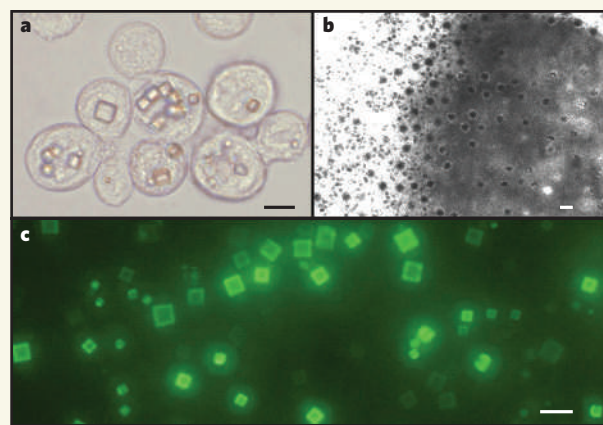


Figure 1 | Intracellular microcrystals. **a**, Insect cells of the Sf21 cell line infected with a recombinant baculovirus expressing the CPV polyhedrin gene. Cubic crystals are evident inside the cells. **b**, Transmission electron micrograph of a polyhedron recovered from a CPV-infected cell. The crystal (dark grey) has many CPV particles visible at the surface. Virions are included throughout the volume of the polyhedron, not just at the surface. **c**, Sf21 cells co-infected with two recombinant baculoviruses, one carrying the CPV polyhedrin gene and the other the gene encoding green fluorescent protein fused with the sequence for the amino-terminal segment of the CPV outer protein VP3. This latter observation points to potential applications in nanotechnology. Scale bars, 20 µm (**a**, **c**) and 0.1 µm (**b**). (Photos courtesy H. Mori, Protein Crystals Corp., Kyoto Inst. Technol., Japan.)